Field demonstration of a scanning lidar and detection algorithm for spatially mapping honeybees for biological detection of land mines

Erik S. Carlsten,[1] Geoffrey R. Wicks,[2,*] Kevin S. Repasky,[3] John L. Carlsten,[2] Jerry J. Bromenshenk,[4] and Colin B. Henderson[4]

[1]Computer Science, EPS Room 357, Montana State University, Bozeman, Montana 59717, USA, 406 994-7828 (ecarlste@gmail.com)

[2]Physics Department, EPS Room 264, Montana State University, Bozeman, Montana 59717, USA, 406 994-6176 (carlsten@physics.montana.edu)

[3]Electrical and Computer Engineering, Cobleigh Hall Room 610, Montana State University, Bozeman, Montana 59717, USA, 406 994-6082 (repasky@ece.montana.edu)

[4]University of Montana, Missoula, Montana 59812, USA

*Corresponding author: wicks.geoffrey@gmail.com

Received 14 October 2010; revised 3 February 2011; accepted 7 February 2011; posted 7 February 2011 (Doc. ID 136591); published 9 May 2011

A biological detection scheme based on the natural foraging behavior of conditioned honeybees for detecting chemical vapor plumes associated with unexploded ordnance devices utilizes a scanning lidar instrument to provide spatial mapping of honeybee densities. The scanning light detection and ranging (lidar) instrument uses a frequency doubled Nd:YAG microchip laser to send out a series of pulses at a pulse repetition rate of 6.853 kHz. The scattered light is monitored to produce a discrete time series for each range. This discrete time series is then processed using an efficient algorithm that is able to isolate and identify the return signal from a honeybee in a cluttered environment, producing spatially mapped honeybee densities. Two field experiments were performed with the scanning lidar instrument that demonstrate good correlation between the honeybee density maps and the target locations.

OCIS codes: 280.3640, 280.0280, 120.0280, 120.4640.

1. Introduction

Unexploded ordnance devices (UXOs) have resulted in a humanitarian crisis with over 50×10^6 UXOs deployed in approximately 90 countries [1]. UXOs kill or injure an estimated 15,000–20,000 people each year [1]. UXOs also remove land from agricultural production, intensifying the humanitarian crisis they cause. The ability to effectively and safely detect unexploded UXOs as a first step in the removal process is an important goal and is driving many research efforts.

Several methods of UXO detection are currently used for demining applications. One of the most common methods of UXO detection involves the use of handheld metal detectors [1]. These devices are swept over the suspected minefield by a human operator, putting the operator at risk. These devices also result in a large number of false positives, because they will detect any buried metal. Furthermore, these devices will not successfully detect UXOs made from plastic or plasticlike materials, which can result in missed targets. A second method used to locate unexploded UXOs is the use of trained

0003-6935/11/142112-12$15.00/0

dogs. Dogs have an excellent sense of smell that is capable of detecting the chemicals associated with UXOs. Dogs have a sensitivity to 2.4 dinitrotolulene (2.4 DNT), a common element in UXOs, of 10^{-8} g/ml [2]. While the use of dogs as a biological detection method of UXOs is well established, dogs are expensive to train, have a short working time, and the dog and handler must still operate in the field, putting both at risk.

Bromenshenk *et al.* are developing a novel biological detection scheme for locating the chemical vapor plumes associated with UXOs utilizing the natural foraging behavior of honeybees [3–6]. Bromenshenk *et al.* have shown that honeybees can detect 2.4 DNT at vapor densities below 50 parts per trillion (ppt) with less than 2% probability of either a false positive or negative when the honeybees are properly conditioned [5]. This conditioning is achieved within two days using automated feeders. Initially, the feeders are located in close proximity to the bee colony, which is made up of several hives. These feeders pump syrup from a storage reservoir into an open dish, providing a rich food source for the bees. This food source contains the scent of the chemical vapor plume, so that bees begin to associate the scent of the chemical vapor plume with a food source. The feeders are then moved away from the bee colony, forcing the bees to begin foraging to find the feeders. At this point, microcontrollers begin to toggle the feeder pump outputs in a random fashion, forcing the honeybees to continue foraging. Because the honeybees have been conditioned to associate the scent of the chemical vapor plume with a rich food supply, they will spend greater periods of time where the chemical vapor plume from the UXOs is strongest [7]. Standoff detection techniques can then spatially map the honeybee densities to provide a map of the chemical vapor plumes associated with the locations of the unexploded UXOs.

An initial experimental demonstration of the use of honeybees to map the chemical vapor plume of buried UXOs was reported by Shaw *et al.* [7]. Honeybees were conditioned and then allowed to forage over a demining test site containing buried targets. A scanning lidar was used to spatially map the honeybee densities over a field of mown grass, and good correlations were demonstrated between the honeybee density and the chemical vapor plumes resulting from the buried targets. The scanning lidar used in this experiment was a modified atmospheric lidar that was not eye-safe and was unable to discriminate between returns associated with honeybees and returns resulting from vegetation.

A low-power scanning lidar system was developed by Hoffman *et al.* for spatial mapping of honeybees [8,9]. This lidar instrument utilized a microchip laser with a pulse repetition rate of 7.2 kHz that was capable of creating a discrete time series of the scattered light for each angle and range bin. These discrete time series were then processed via Fourier analysis. Hoffman *et al.* were able to demonstrate that the modulated light scattered from the wing motion of the honeybee produced a peak in the discrete Fourier transform of the scattered light in the 200–300 Hz frequency range [8,9]. The data processing algorithm, however, performed extremely slowly (13 s per angle bin), and was only able to distinguish between stationary vegetation and honeybees. The ability to discriminate the scattered returns of honeybees from those of moving vegetation is a necessary system capability for the successful detection of UXOs using this method. Foraging honeybees that are searching for a food source fly near the top of the vegetation. If a scanning lidar instrument is to successfully map honeybee densities in an uncontrolled setting, it must be able to separate the return signals from vegetation and honeybees.

In this paper, a scanning lidar instrument similar to that described by Hoffman *et al.* is used during two field experiments to map honeybee densities over unprepared fields containing targets [8,9]. An efficient algorithm developed for processing the large amounts of data collected from the scanning lidar is described in this paper and is applied to the data collected from two field experiments. Good agreement between the algorithm-generated honeybee density map and the target locations is demonstrated, indicating the success of the scanning lidar instrument and the novel data processing algorithm to spatially map honeybee densities in a cluttered environment.

This paper is organized as follows: In Section 2, a description of the scanning lidar instrument and data collection technique is described; in Section 3, the development of the data processing algorithm is discussed; in Section 4, two field experiments are discussed; and in Section 5, some brief concluding remarks are presented.

2. Instrument

A schematic of the scanning lidar instrument used for spatially mapping honeybee densities is shown in Fig. 1. A frequency doubled, passively *Q*-switched diode pumped pulsed microchip Nd:YAG laser (JDS Uniphase NG-10320-100, JDS Uniphase Corp., USA) is used as the laser source for the lidar transmitter. The microchip laser produces greater than 3 μJ of pulse energy with a pulse duration of less than 0.9 ns and a 6.853 kHz pulse repetition frequency. The output from this laser is expanded and recollimated producing a 5 cm diameter beam. The expanded beam is incident on a dielectric beam sampler that transmits 5% of the incident light onto a fast photodiode that is used to trigger the data acquisition. The reflected light is incident on a dielectric steering mirror, allowing field-of-view alignment, and is finally directed to the field using a 20.3 cm × 40.6 cm scanning mirror. This mirror is mounted on a computer-controlled goniometer stage (Zaber LMG60, Zaber Technologies, Inc., Canada) that allows vertical scanning. The mirror and goniometer are then mounted on a computer-controlled

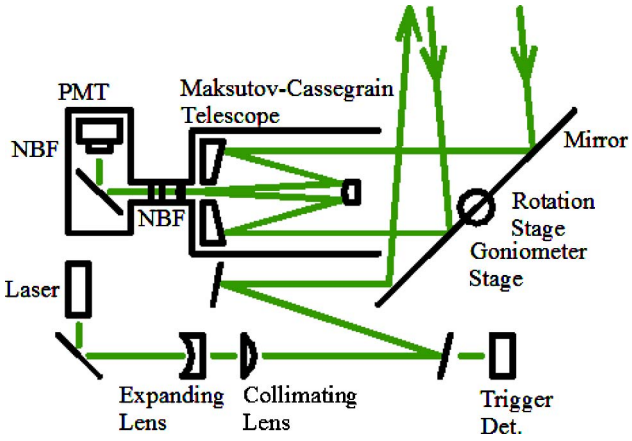

Fig. 1. (Color online) A schematic of the lidar instrument used to spatially map honeybee densities. Pulses from the microchip Nd:YAG laser are sent to the field using the scanning mirror. Returns from the field are collected using a telescope and fed to a PMT after passing through two NBFs.

rotational stage (Zaber LMR58) that allows horizontal scanning. Using a pulsed laser source with the horizontal rotation and goniometer stages allows for 3 degrees of freedom with the instrument, providing the opportunity to resolve the distance to the target (defined as the range bin), the horizontal angle wedge in which the target lies (defined as the angle bin), and the vertical angle wedge in which the target lies (defined as the layer), respectively. For convenience, the range bin, angle bin, and layer of a measurement will be referred to as the location of that measurement, and a scan is completed once a measurement has been taken for each location. The lidar receiver utilizes a commercial 10.2 cm diameter Maksutov–Cassegrain telescope to collect the scattered light. The light from the telescope passes through a collimating lens and narrowband filter (NBF) combination, is reflected from a turning mirror, passes through a second NBF, and is incident on a photomultiplier tube (PMT) module (Hamamatsu H9305-04, Hamamatsu Photonics K.K., Japan). The two NBFs are laser-line filters for the frequency-doubled Nd:YAG with bandwidths of 1 nm. The two NBFs provide adequate filtering of the background light over the operating wavelength range of the PMT.

Data are collected with the scanning lidar instrument in the following manner. The user defines the initial positions of the rotational and goniometer stages (i.e., the initial beam location), the number of laser pulses to be recorded per angle bin (i.e., the temporal resolution), the number of angle bins per layer (i.e., the horizontal angular resolution), the vertical angular resolution, the number of layers per scan, and the number of scans using custom data acquisition software written in the LabVIEW (National Instruments Corp., USA) programming environment. Once these parameters are specified, the scanning mirror is positioned, the laser is enabled, and the data acquisition process begins. Each laser pulse is seen by the trigger detector, which initiates data acquisition. The analog PMT voltage signal is then converted to a discrete time series using a 14 bit analog-to-digital card with a 200 MHz sampling rate (Gage CS14200, Gage Applied Sciences, Inc., Canada). This sampling rate corresponds to a 5 ns timing resolution, which establishes a range bin size of 0.75 m. For each laser pulse, the return signals from up to 140 range bins (700 ns) are collected, corresponding to a maximum operational range of 105 m. The pulse repetition frequency of the laser is 6.853 kHz, corresponding to a temporal pulse separation, and therefore time series resolution, of 146 μs. Once the specified number of pulses has elapsed, the discrete voltage signal as a function of time is recorded in a two-dimensional matrix (2D) for each range bin. These 2D matrices are then organized by range bin to create a three-dimensional (3D) matrix of values for the first angle bin. A graphical representation of the data for one angle bin where a honeybee was detected is given in the upper gray-scale plot in Fig. 2. The discrete time series for range bin 49 of this matrix, illustrating the return signal resulting from the honeybee crossing the beam (as will be discussed in Section 3), is shown in the lower plot of Fig. 2. Once the 3D angle bin data have been recorded, the rotational stage advances the scanning mirror to the next angular position and the angle bin data acquisition process is repeated for the second angle bin. The angle bin data acquisition process is repeated for the specified number of angle bins, completing the first layer of the scan. Once the signal data have been recorded for the first layer, the goniometer then advances the scanning mirror to its next specified vertical angular position and the entire layer process is repeated for the second layer. The layer process is repeated for the specified number of layers, producing one complete scan. The entire scanning process is then repeated for the specified number of scans.

3. Data Processing

Because of the large amount of data collected by the lidar instrument, it is imperative that the data processing software perform efficiently. Also, the software must be able to distinguish four classes of return signals, namely noise, DC, modulated DC, and bee hits. The noise class obtains when the return signal for a particular location is exclusively due to light scattered by airborne particulates. A representation of this class of returns is shown in the range bin (proportional to distance) versus laser pulse number (proportional to time) gray-scale plot given in Fig. 3(a). The DC class of return signal is produced by a stationary rigid scattering target, such as a tree, and is characterized by the appearance of a significant return for all pulses in a particular location. An example of the DC class is shown in range bin 106 of the gray-scale plot in Fig. 3(b). The modulated DC returns can result from vibration of the scanning mirror, beam steering resulting from atmospheric

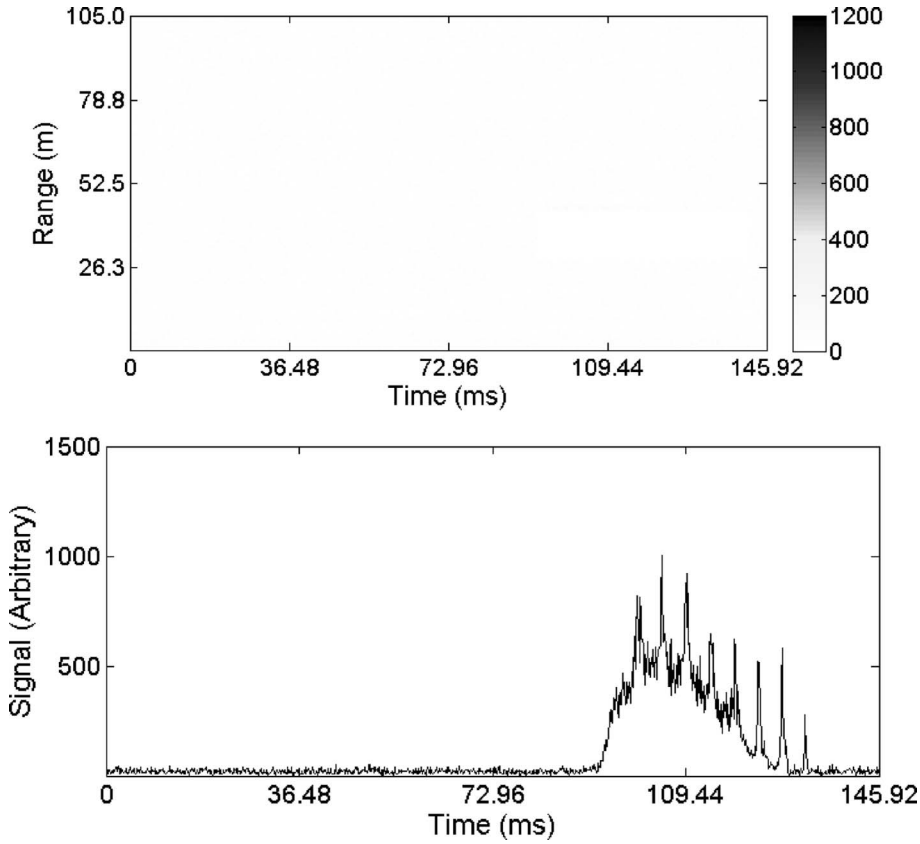

Fig. 2. The upper plot shows the return signal as a function of the range bin number and laser pulse number for a single angle bin. The range on the y axis is found by multiplying the range bin number by the range resolution of 0.75 m, while the time on the x axis is found by multiplying the laser pulse number by 140 μs. The lower plot shows the return signal as a function of time for range bin 49.

turbulence, or vegetation moving in the wind. An example of the modulated DC class is given in range bin 47 of the gray-scale plot in Fig. 3(c). In this case, the object is oscillating at 33 Hz. The bee hit class results from light scattered from honeybee wings, and is characterized by a modulated return signal, the duration of which is determined by both the laser transmitter beam diameter and the honeybee flight velocity. This signal modulation, due to the honeybee wing oscillation and observable in the lower plot of Fig. 2, is in the 200–300 Hz frequency range. This is well below the Nyquist frequency of 3.4265 kHz associated with the 6.853 kHz pulse repetition frequency of the microchip laser [10]. A gray-scale plot demonstrating an example of this signal class is given in Fig. 3(d). Notice that this bee hit is weaker than that given in the lower plot of Fig. 2, as evidenced by the lack of observable fine features. The noise and DC classes of signals are easy to distinguish from the bee hit class of signals. However, differentiation between the modulated DC and bee hit classes of signals requires more filtering.

To understand how the data processing proceeds, a closer look at the discrete voltage signal in both the time and Fourier domain is required. A voltage plot as a function of time is shown for the noise, DC, modulated DC, and bee hit classes in Figs. 4(a)–4(d). Discrete Fourier transforms for the DC, modulated DC, and two bee hits are shown in Figs. 5(a)–5(d). The noise class is characterized by low voltage amplitude as a function of laser pulse number. The Fourier signal of this noise class is flat and is not shown in Fig. 5. The DC class is characterized by a high voltage value and a Fourier signal that starts high, falls off linearly until approximately 200 Hz, and then remains relatively constant, as seen in Fig. 5(a). The modulated DC class is characterized by a modulated voltage signal that reaches a high peak voltage value and has a Fourier signal with significant low-end frequency components as shown in Fig. 5(b). In the case of a strong modulated DC signal (not shown), higher harmonics of these low-end frequency components are evident, lending to the difficulty in distinguishing between a weak bee hit [Fig. 5(c)] and a strong modulated DC signal. The bee class is characterized by a lower peak voltage signal as compared to the DC and modulated DC return signals. The Fourier signal of the bee class shows higher intensity values, between 200–300 Hz. Strong bee hits, produced by an increased duration in the beam or location nearer the transmitter, also show the higher harmonics, evident in Fig. 5(d).

Bee density maps are produced through a series of four processing steps in the MATLAB programming environment. After each step is completed, a false color plot is displayed in the data processing

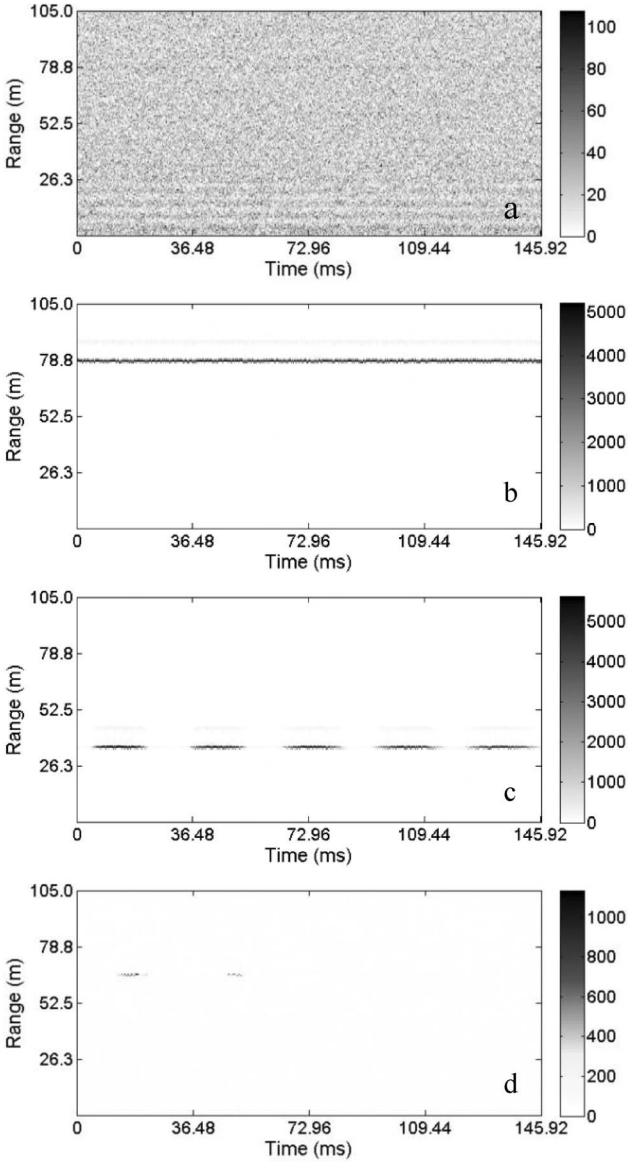

Fig. 3. Return as a function of the range bin and laser pulse number for the four signal classes. (a) Typical noise signal, (b) typical DC return signal, (c) typical modulated DC return, (d) typical return signal from a bee. As shown by the sidebars, each of these plots is scaled differently in order to illustrate the features of each class of signal.

graphical user interface (GUI) developed for this scanning lidar instrument. The first data processing step, shown schematically in Fig. 6, averages the voltage signal over the laser pulse number for each location and is easily handled by MATLAB's matrix manipulation abilities.

The second data processing step, referred to as thresholding, filters out the noise and DC signals, and is achieved in the following manner. For each scan, the average voltage for each location is divided by the average voltage for the corresponding location over all scans. If a DC return signal is present in all of the scans, then the average voltage for one scan will be approximately equal to the average voltage over all scans, so the ratio will be approximately 1. This same argument holds for the noise. However, if a bee hit is evident in several, but not all, scans, then the average voltage signal(s) for the location(s) in which the bee is located for the scan(s) during which the beam and the honeybee are colocated will be greater than the corresponding location voltage average(s) over all of the scans, making the ratio greater than 1. If the ratio is larger than a set threshold value, then the location and scan are marked for further processing. This completes the second step of the data processing. This step greatly reduces the amount of data that needs to be processed in the remaining steps.

The second data processing step efficiently removes the noise and DC classes of signals from the data that needs to be processed further. However, differentiating the modulated DC and bee hit classes requires another operation. The third data processing step uses the fact that the average voltage signal for modulated DC returns is generally larger than the average voltage signal resulting from bees, due to both higher intensity scattering and more time spent in the beam. The third data processing step simply allows the user to set an upper limit on the average voltage. If the average voltage for any location is above this cutoff value, then the return signal is assumed to be of the modulated DC variety. If the average voltage value is below the user-defined cutoff, the location and scan are marked for further processing. This further reduces the amount of data to be analyzed in the fourth data processing step.

The fourth data processing step performs a discrete Fourier transform on all of the data that has passed through the previous three steps. Once the Fourier transform is complete, three values are queried: the maximum value of the Fourier transform in the frequency range of 190–310 Hz (honeybee wing oscillation frequency range); the minimum value between 100 Hz and the frequency corresponding to the maximum value (the lower minimum Fourier value); and the minimum between the frequency corresponding to the maximum value and 350 Hz (the upper minimum Fourier value). Ratios are taken of the maximum Fourier value in the 190–310 Hz frequency range to both the upper and lower minimum Fourier values, and if both ratios are greater than a user-defined threshold, the return signal is determined to be caused by a bee, and a point is placed on the honeybee density map at the corresponding location. The efficiency of this four-step process is greatly increased by the data filtering performed in steps two and three, by significantly reducing the number of discrete Fourier transforms to be performed. As an example, this algorithm requires less than 1 s to perform measurements for an entire angle bin, as compared to approximately 13 s per angle bin using the software developed for Hoffman's experiment.

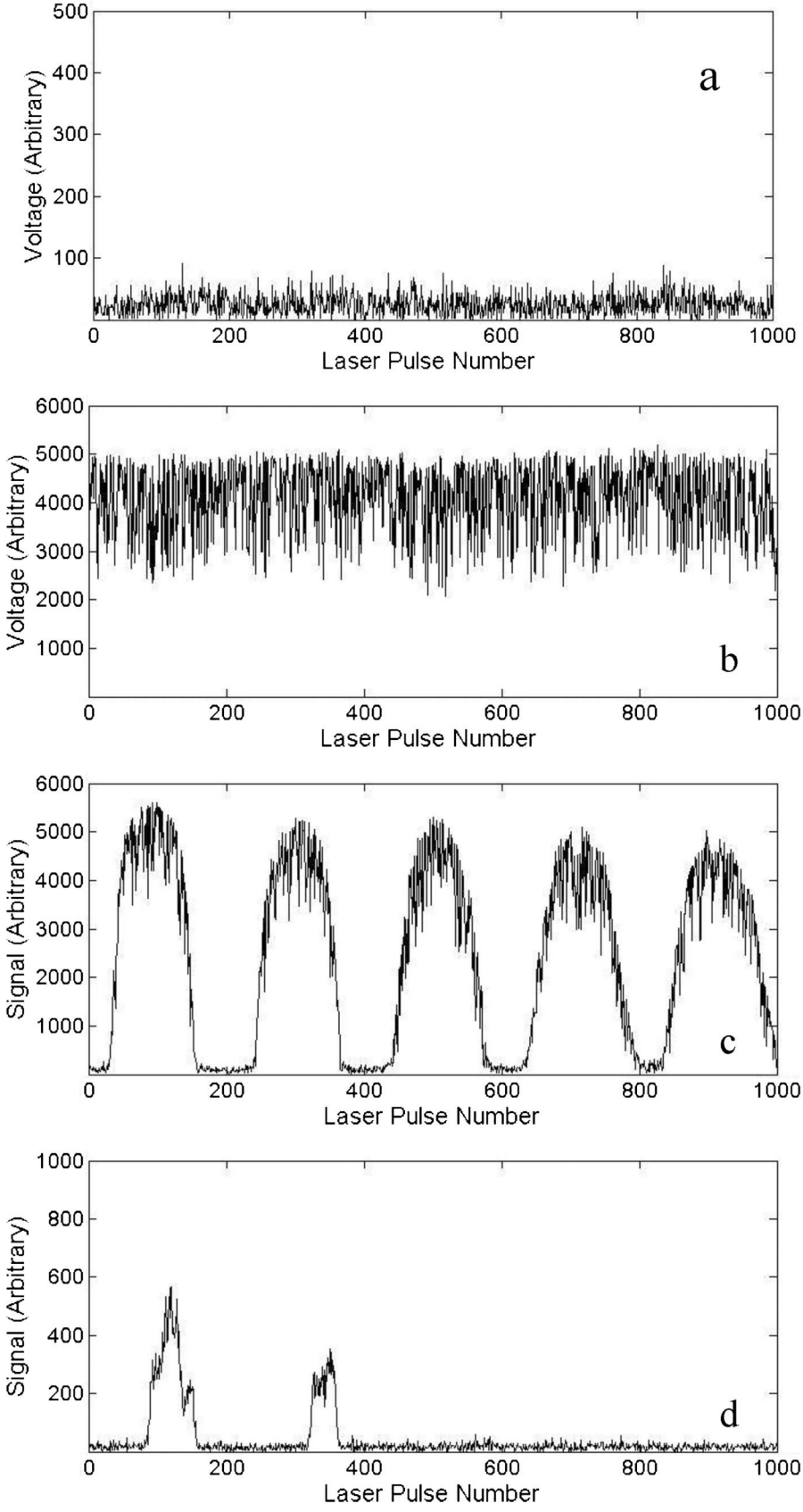

Fig. 4. A plot of the discrete return signal as a function of time for the four classes of return signal. (a), (b), (c), (d) time-dependent return signal for the noise, DC, modulated DC, and bee classes, respectively.

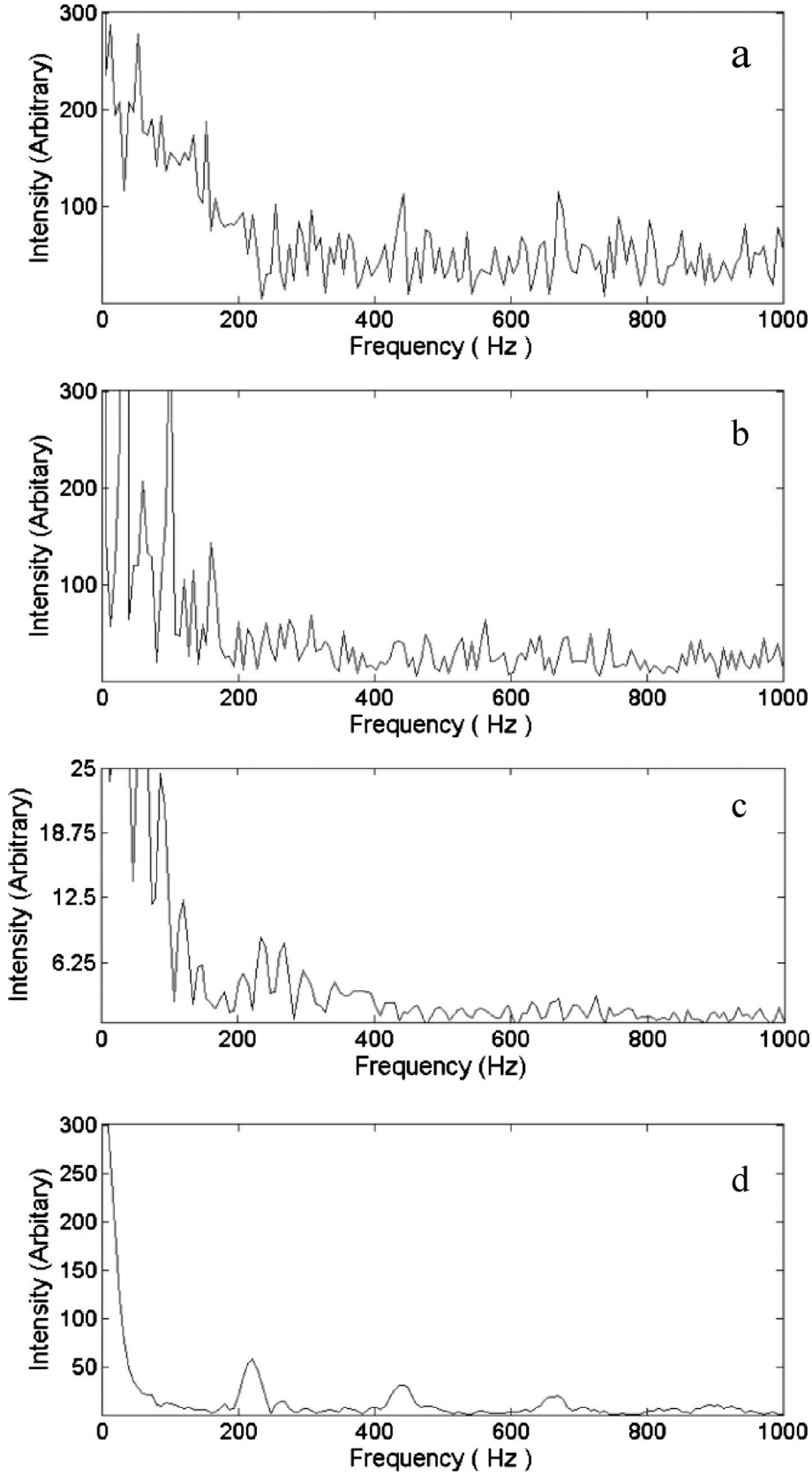

Fig. 5. Discrete Fourier transforms for the signals observed in 4(b) (DC), 4(c) (modulated DC), 4(d) (average bee return), and the lower plot in Fig. 2 (strong bee return), respectively.

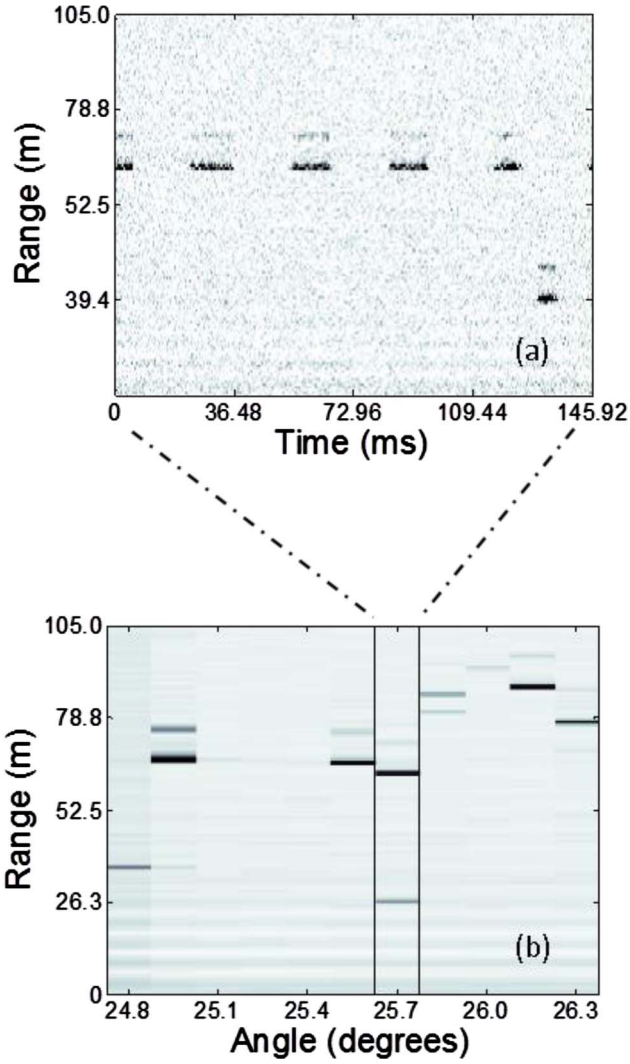

Fig. 6. (Color online) (a) Plot of range bin versus laser pulse number, which represents the collected data for one angle bin. During the first data processing step, the data from each angle bin is compressed by averaging across laser pulse numbers. Each angle bin is then placed into the appropriate column in (b) range bin versus angle bin plot. Plot in (b) represents the average signal seen for one scan across the target field.

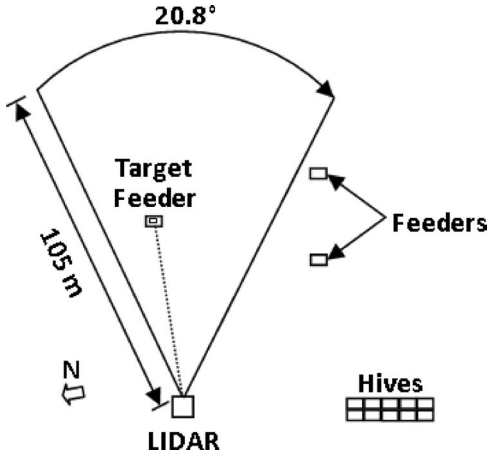

Fig. 7. A schematic of the experimental setup used for the Missoula, Montana, field experiment (target feeder location to scale, hives and external feeder locations approximate). The feeder footprint is 0.023 m × 0.023 m.

4. Field Experiments

Two field experiments were performed to test the capabilities of the scanning lidar for producing bee density maps. The first experiment was performed in Missoula, Montana, and the second experiment was performed in St. George, Utah. During the Missoula, Montana, field experiment, the average low and high temperatures were 1 °C and 18 °C, respectively, the average wind speed was 2.4 m/s, and the average relative humidity was 51%. During the St. George, Utah, field experiment, the average low and high temperatures over the four days of scanning were 6 °C and 22 °C, respectively, the average wind speed was 1.3 m/s, and the average relative humidity was 40%. The weather conditions onsite determine whether or not the bees will forage for food [11]. For both experiments, data were collected between approximately 11:00 a.m. and 6:00 p.m. local time, when the bees were most active, and the honeybees used for the experiments were local species.

A schematic of the experimental setup for the Missoula, Montana, field experiment is shown in Fig. 7. Two feeders were placed approximately 100 m northeast of the beehives. These feeders are computer-controlled and pulse the syrup with the scent of the target to condition the honeybees to associate the scent of the target with food. For this experiment, a feeder was utilized as a target because the honeybees had not yet been conditioned to detect DNT. The target feeder was placed approximately 150 m north of the feeders. The lidar instrument was scanned over the field using the maximum 140 range bins, 1000 laser pulses for each angle bin, 120 angle bins, and one layer for each scan, chosen such that the beam was horizontal and coincided with the top of the vegetation, in order to maximize the number of detected bees, as described in the introduction to this paper. The total angle over which the instrument was scanned was 20.64 deg with an angular step size of 0.1734 deg. A total of 167 scans were completed and the data were processed using the four steps discussed in the previous section. The large number of scans is required in order to maximize the accuracy of the data processing steps, due to the averaging that is performed, and approximately 3.5 h elapsed during data acquisition. Processing the data collected during the Missoula, Montana, field experiment required 2 min 33 s.

A screen capture showing the processed data from the GUI for this field experiment is shown in Fig. 8, where the vertical axis corresponds to the range bin and the horizontal axis corresponds to the angle bin. The upper left-hand plot shows the average voltage return for each location over all 167 scans. The large values seen at approximately range bin 90 between angle bins 10 and 30 result from both DC and modulated DC returns due to vegetation. Note that the large returns from the vegetation mask the signal

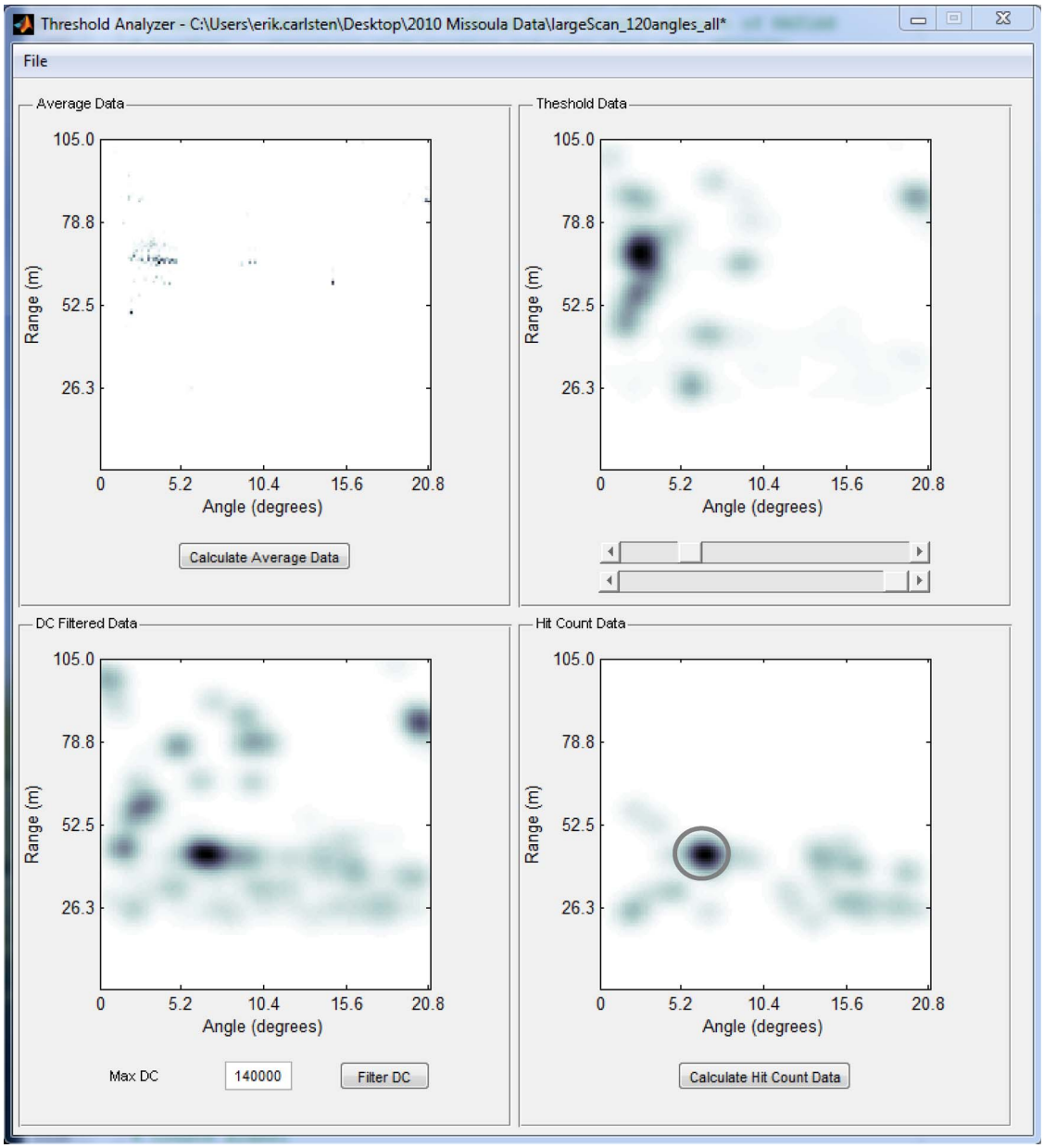

Fig. 8. (Color online) Screen capture of the GUI used to analyze the data collected by the scanning lidar instrument during the Missoula, Montana, experiment. Top left, range bin returns averaged (step 1); top right, lower thresholding performed (step 2); bottom left, upper thresholding performed (step 3); bottom right, Fourier transforms taken and filtered (step 4).

over the single target located in the scanned field at range bin 58 and angle bin 40. The upper right-hand plot in Fig. 8 shows the data after the threshold step is used to filter out the DC and noise returns. The slide bar below this figure allows the user to dynamically adjust the threshold value to complete this processing step. During this step of the data processing, if the return signal from a particular location passes through the threshold filter, then a score of 1 is recorded for this location in a scoring matrix. The data displayed in this plot result from a sliding window Gaussian spatial filter of this score matrix. Note that the modulated DC returns from vegetation near range bin 90 and angle bin 20 still suppress the target feeder location.

The third step, designed to remove modulated DC signals, involves the filtering of the averaged voltage signal by setting an upper threshold value. The user enters the threshold value in the GUI in the box located below the lower left plot in Fig. 8. The return signals that pass this data processing step are used to generate a new score matrix, and a sliding Gaussian spatial filter is used to generate a density map. This step removes most of the modulated DC return signals, leaving mostly return signals from bees. The target feeder, located at range bin 58 and angle bin 40, begins to be evident in this plot.

The fourth data processing step includes performing discrete Fourier transforms on the data that has been filtered by the previous two steps. The results of

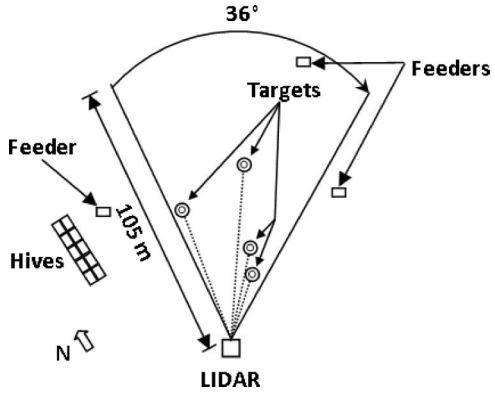

Fig. 9. Schematic of the experimental setup used for the St. George, Utah, field experiment (target locations to scale, hives and feeder locations approximate). The feeder footprint is 0.023 m × 0.023 m, and the DNT target footprint is 0.010 m × 0.010 m.

this Fourier transform analysis are used to generate a final score matrix, and the sliding Gaussian spatial filter is used to produce a density map of the score matrix, and thereby locate the target feeder, indicated by a circle at range bin 58 and angle bin 40 in the lower right-hand plot of Fig. 8. The remaining hits seen in this figure are most likely due to honeybees foraging in the field and transiting between the hives and the target feeder.

A second field experiment for testing the ability of the scanning lidar to map honeybee densities was completed in St. George, Utah. A schematic of the experimental setup is shown in Fig. 9. Feeders were located on either side of the field containing the four DNT-charged targets. Vegetation including sage and juniper was present within the scanned field. In particular, large bushes were present beyond range bin 100. The lidar instrument was scanned over a total of 35.86 deg with 240 angle bins with a single layer, chosen similarly to that in the Missoula,

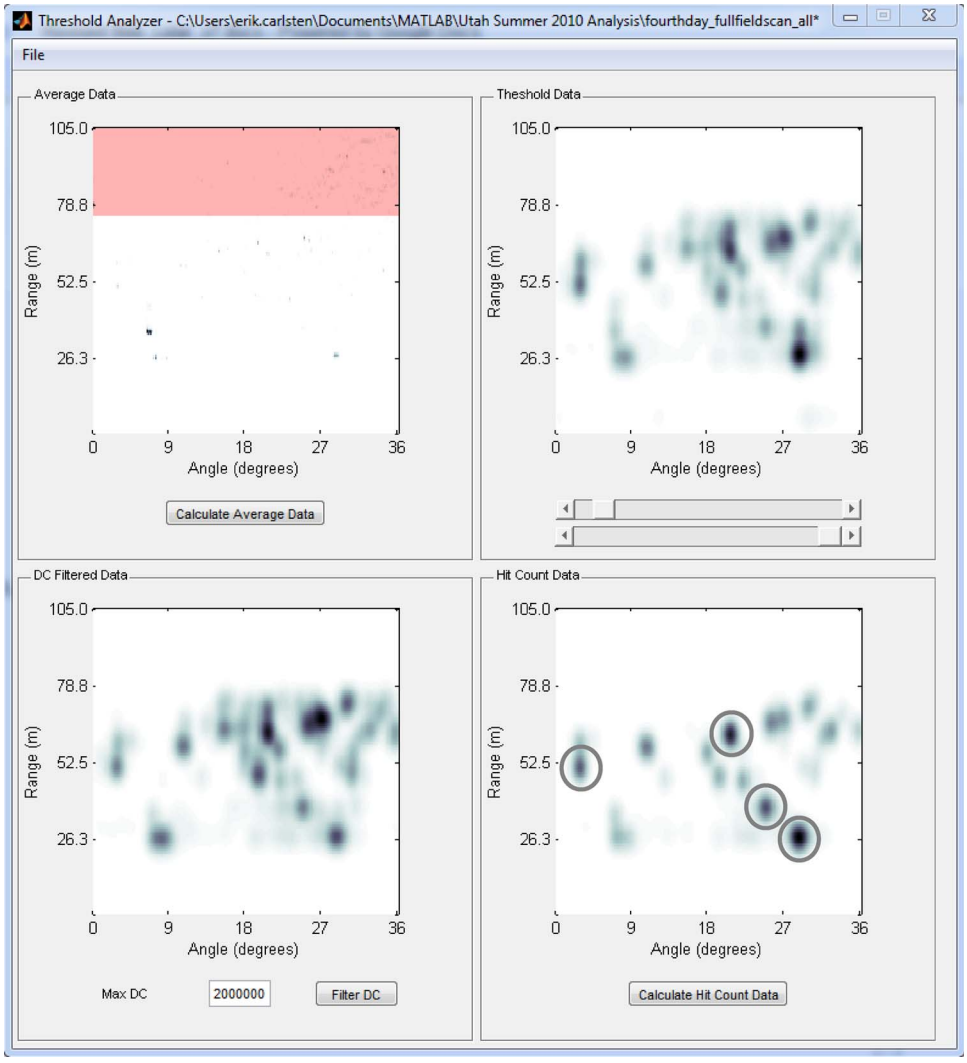

Fig. 10. (Color online) Screen capture of the GUI used to analyze the data collected by the scanning lidar instrument during the St. George, Utah, experiment. Top left, range bin returns averaged (step 1); top right, lower thresholding performed (step 2); bottom left, upper thresholding performed (step 3); bottom right, Fourier transforms taken and filtered (step 4). The four targets are marked by the gray circles in the lower right-hand plot.

Montana, field experiment, and with 1000 pulses per angle bin. A total of 80 scans were performed, which took approximately 3.7 h to complete. The processing of the St. George, Utah, data required 2 min 15 s.

A screen capture of the GUI used to analyze the lidar data from the St. George, Utah, field experiment is shown in Fig. 10. The upper left-hand plot shows the averaged voltage signal as a function of location, with the vertical/horizontal axes corresponding to the range/angle bin, respectively. During this experiment a large number of returns resulted from vegetation beyond range bin 100. To help with this, a new feature was added to the data processing GUI, which allows a user to define the maximum range bin to use for the data remaining three data processing steps. In this data set, the maximum range bin to be analyzed was set to 100; all data beyond range bin 100 is ignored accordingly, which is why the feeder within the angular range of the instrument in Fig. 9 is not evident in the lower right-hand plot of Fig. 10. The data processing steps are identical to those described for the Missoula, Montana, experiment, as is the GUI plot layout. The final map of the score matrix representing returns from bees is shown in the lower right-hand plot of Fig. 10, with the four DNT target locations circled. Good agreement between the bee density map and DNT target locations is seen. However, the bee density map also indicates that bees are seen in other locations in the field, most likely transiting among the feeders, hives, and DNT targets.

It should be noted that the threshold values for data processing steps two and three (2.93 and 10, respectively, for the Missoula experiment, and 1.63 and 10, respectively, for the St. George experiment) were determined by knowing where the feeders were located. In an actual land mine detection scenario, an onsite calibration would need to be performed in order to determine the threshold values to use for that site. More testing and development is necessary to eliminate this inconvenience.

5. Conclusions

The ability to use honeybees' natural foraging behavior for biological detection of land mines is an intriguing idea. Honeybees are available in most areas, and their conditioning can be accomplished in a matter of days. The scanning lidar instrument discussed in this paper provides one potential method for spatially mapping honeybee densities in order to provide a map of the locations of targets such as land mines. A novel data processing algorithm was presented in this paper which provides an efficient method for spatially mapping honeybee densities with the ability to differentiate between honeybee and vegetation lidar returns. Also, the algorithm is able to significantly reduce the time required to process the large amount of data collected by the scanning lidar instrument by utilizing the matrix manipulation capabilities of MATLAB to filter the data before the more time-consuming Fourier analysis is performed. Results from two field experiments were presented that indicate that the scanning lidar instrument, utilizing the novel data processing algorithm, is capable of producing honeybee density maps that successfully locate targets.

The scanning lidar instrument can be improved in three ways. First, the passively Q-switched laser cannot be externally triggered, making it difficult to synchronize the output pulses of the laser with the internal clock on the data acquisition card. This inability to synchronize the laser pulse with the data acquisition card results in an uncertainty in the temporal extent of the pulse propagation, which therefore creates a range uncertainty of up to one range bin, causing a splitting of the voltage signal between two adjacent range bins. When the return signal is split in this manner, the resulting Fourier transforms are not as strongly peaked in the 200–300 Hz window, reducing the signal-to-noise ratio (SNR) of the transform in this frequency range. This makes it more difficult to identify a signal as resulting from a bee, and also to distinguish the modulated DC and bee hit returns. This difficulty could be eliminated by using an actively Q-switched laser that is synchronized with the data acquisition card. Second, a more powerful laser would allow for comparable output intensity, but with a larger beam diameter. This would allow bees to be within the transmitted beam for a longer period of time, resulting in a higher intensity peak in the 200–300 Hz frequency range. This would improve the SNR of the Fourier signal, making it easier to identify bee hit returns. Finally, the inconvenience of having to perform an onsite calibration could be remedied by determining optimal upper and lower threshold values for a variety of weather conditions and using these data to produce preset threshold values that would be automatically implemented based upon the onsite weather.

This work was supported by the U.S. Army RDECOM CERDEC Night Vision and Electronic Sensors Directorate (NVESD) through the contract W909MY-06-C-0037.

References

1. J. MacDonald, J. R. Lockwood, J. McFee, T. Altshuler, T. Broach, L. Carin, R. Harmon, C. Rapaport, W. Scott, and R. Weaver, *Alternatives for Land Mine Detection* (RAND Corp., 2003), available at www.rand.org/publications/MR/MR1608/MR1608.appg.pdf.
2. J. M. Phelan and J. L. Barnett, "Chemical sensing thresholds for mine detection dogs," in Proc. SPIE **4742**, 532–543 (2002).
3. G. C. Smith, J. J. Bromenshenck, D. C. Jones, and G. H. Alnasseer, "Volatile and semivolatile organic compounds in beehive atmospheres," in *Honeybees: Estimating the Environmental Impact of Chemicals*, J. Devillars and M.-H. Pham-Delegue, eds. (Taylor and Francis, 2002), pp. 12–41.
4. J. J. Bromenshenk, C. B. Hendersen, and G. C. Smith, *Biological Systems: Alternatives for Land Mine Detection*, RAND Science and Technology Institute for Office of Sciences and Technology Policy Report, J. MacDonald, J. R. Lockwood, J. McFee, T. Altshuler, T. Broach, L. Carin, C. Rappaport, W. R. Scott, and R. Weaver, eds. (RAND Corp., 2003), available at http://www.rand.org/publications/MR/MR1608.

5. J. J. Bromenshenk, C. B. Henderson, R. A. Seccomb, R. T. Etter, S. F. Bender, P. J. Rodacy, J. A. Shaw, N. L. Seldomridge, and L. H. Spangler, "Can honeybees assist in area reduction and land mine detection?," J. Mine Action 7.3 (2003), available at http://www.maic.jmu.edu/journal/7.3/focus/bromenshenk/bromenshenk.htm.
6. J. J. Bromenshenk, C. B. Henderson, R. A. Succomb, L. H. Spangler, J. H. Shaw, K. S. Repasky, J. L. Carlsten, T. Balch, P. Rodacy, and S. Bender, Technical Report-Study_ Services, CRDL DI-MISC-80598A, for U.S. Joint Chiefs of Staff (U.S. Department of Defense, 2004).
7. J. A. Shaw, N. Seldomridge, D. L. Dunkle, P. W. Nugent, L. Spangler, J. J. Bromenshenk, C. B. Henderson, J. H. Churnside, and J. J. Wilson, "Polarization measurements of honeybees in flight for locating land mines," Opt. Express **13**, 5853–5863 (2005).
8. D. S. Hoffman, A. R. Nehrir, K. S. Repasky, J. A. Shaw, and J. L. Carlsten, "Range-resolved optical detection of honeybees by use of wing-beat modulation of scattered light for locating land mines," Appl. Opt. **46**, 3007–3012 (2007).
9. K. S. Repasky, J. A. Shaw, R. Scheppele, C. Melton, J. L. Carlsten, and L. H. Spangler, "Optical detection of honeybees by use of wing-beat modulation of scattered laser light for locating explosives and land mines," Appl. Opt. **45**, 1839–1843 (2006).
10. A. V. Oppenheim, A. S. Willsky, and S. H. Nawab, *Signals and Systems*, 2nd ed. (Prentice Hall, 1997), pp. 514–581.
11. S. A. Corbet, M. Fussell, R. Ake, A. Fraser, C. Gunson, A. Savage, and K. Smith, "Temperature and the pollinating activity of social bees," in Ecol. Entomol. **18**, 17–30 (1993).